

Flux-Bubble Models and Mesonic Molecules

M.M. Boyce, J. Treurniet, and P.J.S. Watson

Ottawa-Carleton Institute for Physics, Carleton University, Ottawa, Ontario, Canada, K1S-5B6

Abstract: It has been shown that the string-flip potential model reproduces most of the bulk properties of nuclear matter, with the exception of nuclear binding. Furthermore, it was postulated that this model with the inclusion of the colour-hyperfine interaction should produce binding. In some recent work a modified version of the string-flip potential model was developed, called the flux-bubble model, which would allow for the addition of perturbative QCD interactions. In attempts to construct a simple $q\bar{q}$ nucleon system using the flux-bubble model (which only included colour-Coulomb interactions) difficulties arose with trying to construct a many-body variational wave function that would take into account the locality of the flux-bubble interactions. In this paper we look at a toy system, a mesonic molecule, in order to understand these difficulties. *En route*, a new variational wave is proposed that may have a significant enough impact on the old string-flip potential model results that the inclusion of perturbative effects may not be needed.

1 Introduction

For the past 30 years several attempts have been made, with little success, to describe nuclear matter in terms of its constituent quarks. The main difficulty is due to the non-perturbative nature of QCD. The only rigorous method for handling multi-quark systems to date is lattice QCD. However, this is very computationally intensive and given the magnitude of the problem it appears unlikely to be useful in the near future.¹ As a result, more phenomenological

¹ Some very recent advancements have been made in the area of lattice QCD that have reduced computation time by several orders of magnitude. “Now what took hundreds of Cray Supercomputer hours can be done in only a few hours on a laptop

means must be considered.

A good phenomenological model should be able to at least reproduce qualitatively all the overall bulk properties of nuclear matter. In particular,

- nucleon gas at low densities with no power-law van der Waals forces
- nucleon binding at higher densities
- nucleon swelling and saturation of nuclear forces with increasing density
- quark gas at extremely high densities

There are many models that attempt to reproduce these properties but none of them does so completely. In this paper, only the string-flip potential model [2–4], will be considered. This model appears to be promising because it reproduces most of the aforementioned properties with the exception of nucleon binding. In an attempt to find the root of this problem, a toy mesonic molecular system will be used to study the inclusion of perturbative interactions and variational wave functions [5].

1.1 The String-Flip Potential Model

The idea of string-flip potential models is borrowed from certain results in lattice QCD and experimental particle physics. A potential derived from computations in lattice QCD is confirmed by fitting mesonic spectra in particle physics experiments. It has been found that the most phenomenologically satisfactory potential model between quarks and antiquarks has the form

$$V(r) \sim \sigma r - \frac{4}{3} \frac{\alpha_s}{r}. \quad (1)$$

This is basically an interpolation between the long range non-perturbative (σr) and short range perturbative ($-\frac{4}{3} \frac{\alpha_s}{r}$) parts of the force between pairs of quarks (Fig. 1). The string-flip potential model ignores the short range part of the potential and considers an ensemble of quark-antiquark pairs, $q\bar{q}$, such that the total string length, $\sum r_{q\bar{q}}$, is minimal: *i.e.*,

$$V = \sigma \sum_{\min\{q\bar{q}\}} r_{q\bar{q}}. \quad (2)$$

This particular model has been used in an attempt to model nuclear matter. Although it has an obvious shortcoming, in that it is more applicable to a pion gas, it does surprisingly well at predicting some of the overall bulk properties of nuclear matter [3,4].

computer.” [1].

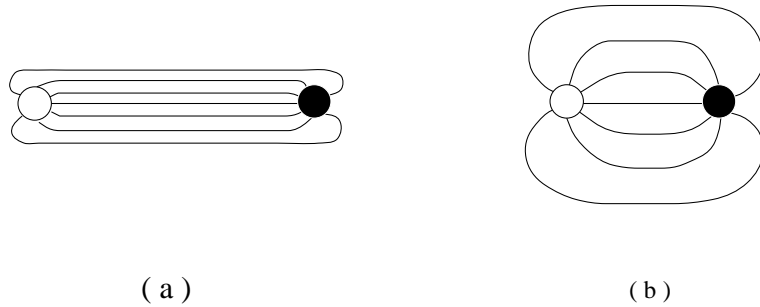


Fig. 1. The colour field lines between quarks collapse upon themselves, due to the self interacting nature of the gluons, to form a flux-tube-like structure. At long distances (a) the fields lines collapse to become almost string-like and at short distances (b) the fields lines expand to become almost QED-like.

It is fairly straightforward to generalize this simple model to a more realistic one which involves triplets of quarks. Here the flux-tubes leaving each quark meets at a central vertex such that overall length, r , of “flux-tubing” is minimized (*cf.* Fig. 2). The potential energy is simply σr [6].

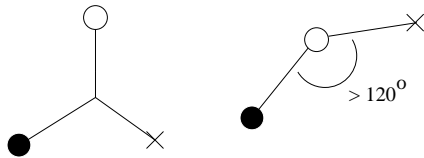


Fig. 2. Flux-tube arrangements for the 3q cluster potentials.

In a more general setting one could consider a full many-body quark potential in which large clusters of quarks may be connected by a single network of flux-tubes [3]; in general, this “gas” is assumed to consist of colourless objects. Again the potential energy is simply σr , where r is now the minimal amount of

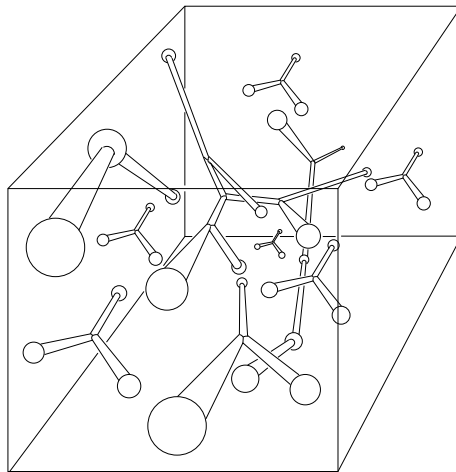


Fig. 3. Possible flux-tube configurations for an $SU_c(3)$ quark gas in a box.

flux-tubing used for a given cluster of quarks. In such a model, there could exist

very complex topological configurations of flux-tubes, such as long strands or web-like structures (Fig. 3).

All of these models are completely motivated by results from lattice QCD, where variations are taken about minimal lattice field configurations between quarks.

Notationally we will refer to these, “linear potential models,” as, “ $SU_\ell(N)$ models,” where the $SU(N)$ refers to the $SU_c(N)$ Yang-Mills gauge group and the subscript, “ ℓ ,” refers to, “linear potential,” [2]. In some models each quark has fixed colour to simplify the searches for minimal flux-tube configurations as the system of quarks evolves. When necessary, for clarity, these models will be referred to as, “ $SU'_\ell(N)$ models.”

1.2 Onward

This paper is divided into three major sections, sandwiched between introduction and conclusions. The first section, is a discussion of the problems faced when attempts were made to extend the string-flip potential model to include perturbative QCD interactions. This is followed by a section on mesonic molecules. It is here, that investigations of the problems faced with the string-flip potential model and its extensions are carried out in detail. The final section reviews all of the findings and their possible consequences for modeling of nuclear matter.

2 The Demise of the String-Flip Potential Model

In some earlier work it was hypothesized that the String-Flip potential model was incapable of producing nuclear binding without the addition of perturbative QCD interactions [2,7]. A model was recently proposed, called the Flux-Bubble Model [7], which allowed the perturbative QCD to be included. In this section we now discuss this model and the difficulties that arise in the implementation of it.

2.1 Flux-Bubble Models

The primary objective is to construct a model which combines both nonperturbative (flux-tubes) and perturbative (one-gluon exchange) aspects of QCD in a consistent fashion. In order to simplify this task only colour-Coulomb

extensions to a linear potential model using $SU(2)$ colour, *i.e.*, $SU_\ell(2)$, will be considered.

The extension of the linear potential model for $q\bar{q}$ pairs is

$$v_{ij} \sim \begin{cases} \sigma(r_{ij} - r_0) & \text{if } r_{ij} > r_0 \\ \alpha_s \lambda_{ij} \left(\frac{1}{r_{ij}} - \frac{1}{r_0} \right) & \text{if } r_{ij} < r_0 \end{cases} \quad \begin{array}{c} \text{V} \\ | \\ \text{Linear} \\ \nearrow \\ \text{Coulomb} \\ \curvearrowright \\ r_0 \end{array} \quad (3)$$

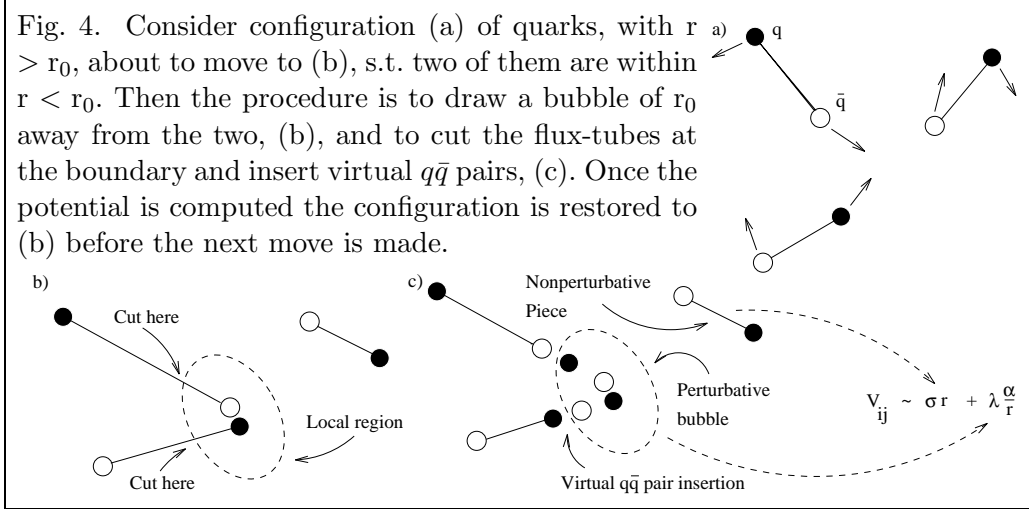
where $\lambda_{ij} = -3/4, 1/4$ for unlike and like colours respectively, and $\alpha_s \approx 0.1$. This is simply a variant of the phenomenological potential,

$$V(r) \sim \sigma r - \frac{4}{3} \frac{\alpha_s}{r}, \quad (1)$$

mentioned in § 1.1; the major difference being that the nonperturbative and perturbative parts are completely separated in the former as opposed to the latter. When the quarks are separated at a distance greater than r_0 the potential is purely linear and when they are inside this radius it is purely Coulomb. In effect, for distances less than r_0 , a “bubble” is formed in which the quarks are free to move around, in an asymptotically free fashion. In both distance regimes the net colour of the system is neutral.

The extension of the linear potential, although simple for a pair of quarks, becomes more complex when considering extensions for many pairs of quarks. In particular, it is difficult to construct a potential model when some set of quarks lie within r_0 , without forming a colour singlet so that they must be connected to more distant quarks by flux-tubes. An *ansatz* that satisfies these requirements is obtained by inserting virtual $q\bar{q}$ pairs across any of the intersection boundaries formed by the flux-tubes with the bubbles. Now the segments of flux-tubes that lie outside the bubbles remain intact while the segments inside simply dissolve; giving the desired result. Fig. 4 illustrates the dynamics of this model. Notice that this model allows the construction of colourless objects because of the insertion of the virtual $q\bar{q}$ pairs. These virtual quarks are used as a tool to calculate the overall length of the flux-tube correctly. They are not used in computing the Coulomb term however, as the field energy is already taken into account by the “real” quarks inside the bubbles. In general, once the bubbles have been determined, the flux-tubes must be reconfigured in order to minimize the linear part of the potential.

Although the model is currently for $SU_\ell(2)$ it should be easy to extend it to a full $SU_\ell(3)$ model with all the one-gluon exchange phenomena.



2.2 In Search of a Wave Function

Fig. 5 shows some preliminary results using the $SU'_\ell(2)$ flux-bubble model described in the previous section. For $r_0 = 0 \text{ fm}$ the Monte Carlo recovers the

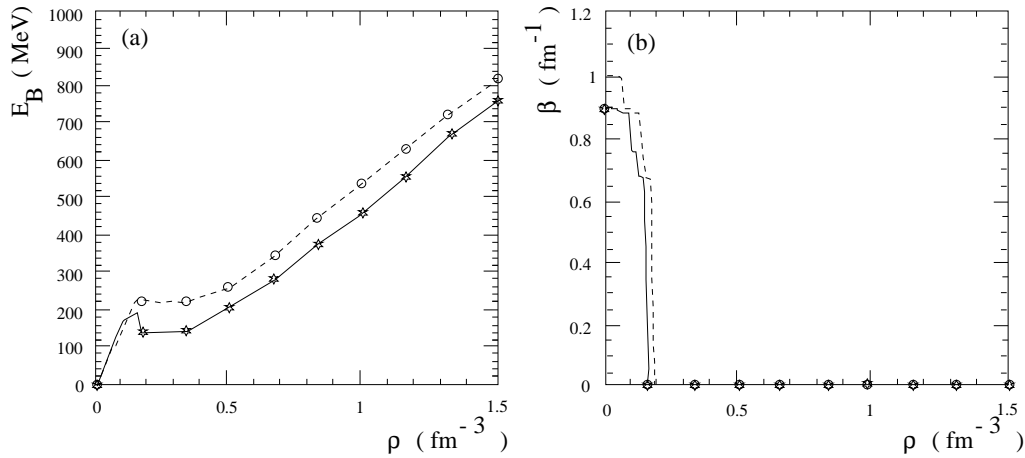


Fig. 5. Binding energy, $E_B(\rho)$ ((a) above), and inverse correlation length, $\beta(\rho)$ ((b) above), as function of density, ρ , for $r_0 = 0 \text{ fm}$ (---) and $r_0 = 0.1 \text{ fm}$ (—), with $m_q = 330 \text{ MeV}$, $\sigma = 910 \text{ MeV/fm}$, and $\alpha_s = 0.1$. These graphs were created by using a coarse 10×10 mesh of points in ρ and β . The minimal curves were extracted by using linear interpolation between the minimum data points on the $E_B(\rho, \beta)$ -mesh surface.

same results for the $SU'_\ell(2)$ string-flip potential model [4], as expected, and for $r_0 = 0.1 \text{ fm}$ the result differs only slightly.

These results are questionable, as the wave function that was used is not ideal.

It consisted of a slight modification to the old $SU_\ell(2)$ wave function [4],

$$\Psi_{\alpha\beta\rho} = e^{\underbrace{-\sum_{\min\{q\bar{q}\}} (\beta r_{q\bar{q}})^\alpha}_{\chi_{\alpha\beta}^{(\text{Linear})}}} \Phi_\rho^{(\text{Fermi})}, \quad (4)$$

in which a new correlation piece, $\chi_{\alpha'\beta}^{(\text{Coulomb})}$, was added to account for the local attractive Coulomb interactions² as they occurred: *i.e.*,

$$\Psi_{\alpha\alpha'\beta\rho} \sim \chi_{\alpha\beta}^{(\text{Linear})} \times \chi_{\alpha'\beta}^{(\text{Coulomb})} \times \Phi_\rho^{(\text{Fermi})}, \quad (5)$$

where

$$\chi_{\alpha'\beta}^{(\text{Coulomb})} = e^{\underbrace{-\sum_{\min\{q\bar{q}\}_+} \{(\beta r_{q\bar{q}})^{\alpha'} \theta(r_0 - r_{q\bar{q}})\}}_{\min\{q\bar{q}\}_+}} \quad (6)$$

with parameters α , α' , β and ρ , such that $\alpha = 1.75$ and $\alpha' = 1$, and where $\sum_{\min\{q\bar{q}\}_+}$ is over $\{q\bar{q}\}$ (*i.e.*, the attractive bits) in the complement of $\sum_{\min\{q\bar{q}\}}$ (*cf.* Eq. (2)). However, because the flux-tubes and bubbles can now be created or destroyed the wave function is, in general, no longer continuous to order $\vec{\nabla}^2$ (*cf.* Eq. (6)), and so a variational lower bound is no longer guaranteed. Therefore, a new wave function is needed, but, it is a rather difficult task to come up with a wave function which takes into account the locality of these flux-bubble interactions, is smooth and continuous, and involves very few parameters.

The aforementioned wave function has two “independent” parameters, ρ and β ; the α ’s were assumed to be fixed. This is in contrast to the previous case for the $SU'_\ell(3)$ model, given in ref. [2], in which ρ and β varied parametrically with a single parameter, θ . The reason this does not apply here is because the flux-bubble potential breaks the scaling transformation

$$(\beta, \rho^{1/3}) \longrightarrow \zeta(\theta) (\cos \theta, \sin \theta), \quad (7)$$

of ref. [2], where $[\zeta(\theta)] \sim fm^{-1}$. This extra degree of freedom greatly increases the computation time.

The results in Fig. 5 were generated on a coarse 10×10 mesh of points, in ρ and β , and required 18hrs of CPU time on an 8 node farm. Clearly this procedure would be ridiculously slow if more parameters were to be added:

$$\tau_{\text{CPU}} \sim \mathcal{O}(R^p) \quad (8)$$

where R is the mesh resolution in each ordinate, and p is the number of parameters.

² The repulsive interactions were assumed to be taken care of by the presence of the Slater wave function, $\Phi_\rho^{(\text{Fermi})}$.

Thus, a way of checking different wave functions and minimization schemes which does not consume large amounts of CPU time is desirable. In particular, a mini-laboratory is needed in which various aspects of the string-flip and flux-bubble potential models, from wave functions to minimization schemes, can be investigated.

3 Mesonic Molecules

An interesting place that might make a good mini-laboratory is a mesonic-molecule [8], Q_2 , consisting of two heavy quarks and two relatively light antiquarks: see Fig. 6. The quarks are assumed to be heavy so that the light

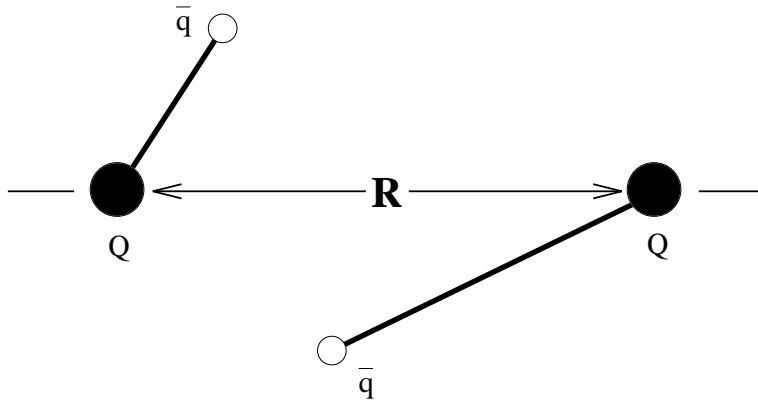


Fig. 6. A mesonic-molecule, Q_2 , with two heavy quarks and two light antiquarks. antiquarks can move around freely without disturbing their positions: *i.e.*, the adiabatic approximation. By varying the distance, R , between the heavy quarks a mesonic-molecular potential, $U(R)$, can be computed.

The Schrödinger equation that describes the effective potential, $U(R)$, is given by [9]

$$\left(\frac{1}{2m_q} \sum_{\bar{q}} \vec{\nabla}_{\bar{q}}^2 + V \right) \Psi = U(R)\Psi; \quad (9)$$

we shall assume $m_q \approx 330 \text{ MeV}$. The potential V describes the many-body nature of the four quark system, and is therefore model dependent. This equation can be solved variationally for $\bar{U}(R)$, at fixed values of R , by guessing at the form the wave function, Ψ , and minimizing

$$\bar{U} = \bar{T} + \bar{V} \quad (10)$$

with respect to the parameters in Ψ . In this paper the expectation values \bar{T} and \bar{V} will be found by using the Metropolis algorithm [2,10], and the optimal parameters for Ψ will be found by using the distributed minimization algorithm [5,11] on $\bar{U}(R)$.

The distributed minimization algorithm was developed to handle the problem of reducing CPU overhead. It involves the usage of several *CPU*'s to perform interlaced parabolic searches for the minima of a given surface. For the Q_2 system this algorithm yields

$$\tau_{\text{CPU}} \sim \mathcal{O}\left(\frac{p}{m}\right), \quad (11)$$

for p parameters and m computers. Similar results are expected for nuclear matter calculations.

The Q_2 system provides a good way of checking potential models for the possibility of nuclear (mesonic) binding. Moreover, because of its simplicity, it allows for checking various wave functions and minimization schemes (*i.e.*, the development of the distributed minimization algorithm) without being too concerned about CPU overhead.

3.1 A General Survey of Extensions to $SU_\ell(2)$

In this section the effects of extending the old $SU_\ell(2)$ [4] model to include flux-bubbles, with and without fixed colour (*i.e.*, $SU_\ell(2)$ and $SU'_\ell(2)$ respectively), will be investigated in the context of the mesonic-molecular system, Q_2 . Here we have decided to consider $SU_\ell(2)$, in a colour-Coulomb setting, instead of $SU_\ell(3)$, for simplicity.

For the old $SU_\ell(2)$ model the variational wave function was assumed to be of the form [4],

$$\Psi_{\alpha\beta} = e^{-\sum_{\min\{Q\bar{q}\}} (\beta r_{Q\bar{q}})^\alpha}, \quad (12)$$

where α and β are variational parameters, and $r_{Q\bar{q}}$ is the distance between a given $Q\bar{q}$ pair. The summation in the exponent of the wave function is over the set of $Q\bar{q}$ pairs that requires the least amount of flux-tubing: *i.e.*,

$$V = \sigma \sum_{\min\{Q\bar{q}\}} r_{Q\bar{q}} \equiv \sigma \min\left\{\sum_{\{Q\bar{q}\}} r_{Q\bar{q}}\right\}, \quad (13)$$

or more explicitly

$$V = \sigma \min\{r_{Q_1\bar{q}_1} + r_{Q_2\bar{q}_2}, r_{Q_1\bar{q}_2} + r_{Q_2\bar{q}_1}\}, \quad (14)$$

cf. Eq. (2). Therefore, the kinetic energy is simply

$$\bar{T} = \frac{\alpha\beta^\alpha}{2m_q} \left\langle \sum_{\min\{Q\bar{q}\}} [\alpha(1 - (\beta r_{Q\bar{q}})^\alpha) + 1] r_{Q\bar{q}}^{\alpha-2} \right\rangle. \quad (15)$$

Now, if we assume for the moment that the colour is affixed to the quarks (*i.e.*, $SU'_\ell(2)$), then the most general flux-bubble potential is of the form

$$V = \sigma \sum_{\min\{Q\bar{q}\}} (r_{Q\bar{q}} - r_0) \theta(r_{Q\bar{q}} - r_0) + \alpha_s \sum_{i < j} \lambda_{p_i p_j} \left(\frac{1}{r_{p_i p_j}} - \frac{1}{r_0} \right) \theta(r_0 - r_{p_i p_j}), \quad (16)$$

with particle index $p_k \in \{Q_i, \bar{q}_j | i, j = 1, 2\}$, such that $k = 1, 2, 3, 4$, and $SU_c(2)$ colour factor

$$\lambda_{p_i p_j} = \begin{cases} -\frac{3}{4} & \text{if } p_i p_j \in \{\bar{q}Q\} \\ \frac{1}{4} & \text{if } p_i p_j \in \{\bar{q}\bar{q}, QQ\} \end{cases}. \quad (17)$$

This potential can be rewritten into the more enlightening form

$$\begin{aligned} V = & \sum_{\min\{q_i \bar{q}_j\}} \left[\sigma (r_{q_i \bar{q}_j} - r_0) \theta(r_{q_i \bar{q}_j} - r_0) - \frac{3}{4} \alpha_s \left(\frac{1}{r_{q_i \bar{q}_j}} - \frac{1}{r_0} \right) \theta(r_0 - r_{q_i \bar{q}_j}) \right] \\ & - \frac{3}{4} \alpha_s \sum_{q_i \bar{q}_j \in \overline{\min\{q_i \bar{q}_j\}}_+} \left(\frac{1}{r_{q_i \bar{q}_j}} - \frac{1}{r_0} \right) \theta(r_0 - r_{q_i \bar{q}_j}) \\ & + \frac{1}{4} \alpha_s \sum_{q_i q_j \in \overline{\min\{q_i \bar{q}_j\}}_-} \left(\frac{1}{r_{q_i q_j}} - \frac{1}{r_0} \right) \theta(r_0 - r_{q_i q_j}), \end{aligned} \quad (18)$$

where $q_i \in \{Q, q\}$. The sets $\overline{\min\{q_i \bar{q}_j\}}_+$ and $\overline{\min\{q_i \bar{q}_j\}}_-$ contain the attractive and repulsive quark pairings, respectively, in the complement ($\overline{\min\{q_i \bar{q}_j\}}$) of the set $\min\{q_i \bar{q}_j\}$: *i.e.*,

$$\overline{\min\{q_i \bar{q}_j\}} = \overline{\min\{q_i \bar{q}_j\}}_+ \cup \overline{\min\{q_i \bar{q}_j\}}_-.^3$$

The two terms inside the square brackets of Eq. 18 represents a linear potential followed by its colour-Coulomb extension: *cf.* Eq. (1). The remaining terms represent the rest of the colour-Coulomb interactions, which contain both attractive and repulsive bits.

Fig. 7 shows the results of the Monte Carlo for the flux-bubble potential and its various terms, given by Eq. (18). The details of the analysis, and hereinafter, can be found in appendix A.

The results of the analysis show that a reduced mass of

$$\mu_Q \gtrsim (53.7 \pm 1.9) \text{ GeV} \quad (19)$$

is required to obtain binding for these potentials. This should not be too

³ *e.g.*, if $\min\{q_i \bar{q}_j\} = \{Q_1 \bar{q}_2, Q_2 \bar{q}_1\}$ then $\overline{\min\{q_i \bar{q}_j\}} = \{Q_1 \bar{q}_1, Q_2 \bar{q}_2, Q_1 Q_2, \bar{q}_1 \bar{q}_2\}$, which implies $\overline{\min\{q_i \bar{q}_j\}}_+ = \{Q_1 \bar{q}_1, Q_2 \bar{q}_2\}$ and $\overline{\min\{q_i \bar{q}_j\}}_- = \{Q_1 Q_2, \bar{q}_1 \bar{q}_2\}$.

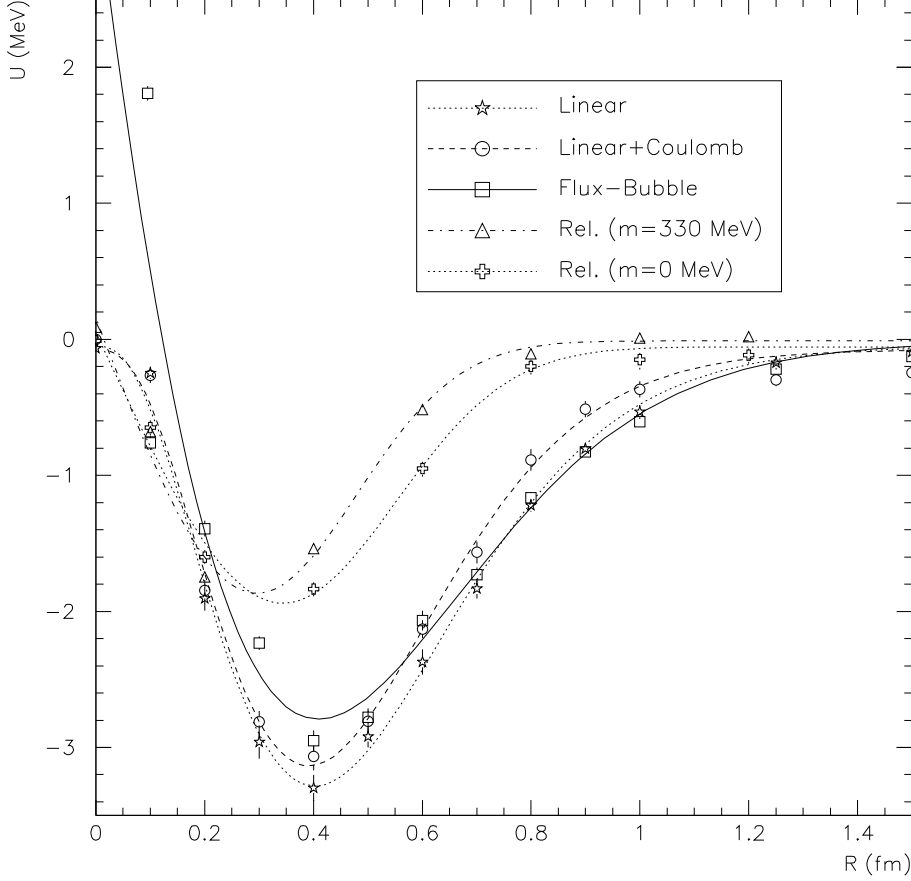


Fig. 7. The binding energy, $E_B(R)$ ($= U(R) - U_\infty$ s.t. $U_\infty \equiv U(\infty)$), for the Q_2 system as function of heavy quark separation for a linear (Eq. (13)), a linear-plus-Coulomb (square brackets of Eq. (18)), and a flux-bubble (Eq. (18)) potential model. Also included, for contrast, are the semi-relativistic results discussed in § 4. The curves in these plots have been parameterized by $u(r) \sim u_0 \{ e^{-2\kappa b(r-r_0)^a} - 2\kappa e^{-b(r-r_0)^a} \} (r - \varepsilon)^\eta$ (cf. Morse potential [9,12]).

surprising as the potential wells are quite shallow,

$$\bar{D} \approx 2.986 \pm 0.030 \text{ MeV}. \quad (20)$$

It is interesting to investigate whether or not the string-flip potential models, represented by Eq. 18, actually mimic pion exchange. Therefore, the asymptotic parts of the $\bar{U}(R)$'s were fitted to Yukawa potentials. The results of the analysis yielded an exchange mass of

$$\bar{m}_{\text{ex}} \approx (636 \pm 41) \text{ MeV}, \quad (21)$$

which is about 4.5 times too big.

Finally, the flux-bubble potential is extended to allow the colour to move around. The potential is similar to that of Eq. 18 except now the particle indices, p_k , carry colour degrees of freedom:

$$\begin{aligned} q_k \in \{R_i, \bar{B}_i, r_i, \bar{b}_i | i = 1, 2\} &\subseteq SU_c(2), \\ \bar{q}_k \in \{\bar{R}_i, B_i, \bar{r}_i, b_i | i = 1, 2\} &\subseteq \overline{SU_c(2)}, \end{aligned}$$

i.e.,

$$b \sim \bar{r}, \dots, \text{etc.} \Leftrightarrow SU_c(2) \sim \overline{SU_c(2)},$$

where the capital case letters represent the heavy quarks, the lower case letters represent the light quarks, the letters r and R represent the red quarks, and the letters b and B represent the blue quarks. Therefore, the $\min\{Q\bar{q}\}$ in Eq. 18 is determined by Eq. 13 such that colour is no longer fixed to a given quark. Fig. 8 shows the results of the Monte Carlo for this potential.

One of the most noticeable peculiarities of Fig. 8 is the apparent linearity inside the potential. In fact, a linear fit to this region (see the insert in Fig. 8) yields a slope of $(909.8 \pm 1.0) \text{ MeV}/fm$! This corresponds to the linear potential $U \sim \sigma R$. A more subtle feature is at the origin where the potential starts to plummet to $-\infty$. This region is due to the coulomb attraction between the two heavy quarks. Out near $R = 1 \text{ fm}$ there appears to be a barrier and beyond this no more structure. Therefore, as two mesons, each containing a heavy quark and a light anti-quark, are brought together from infinity they feel a repulsive force. When near enough, flux-tubes are exchanged, and the two mesons dissociate into one meson containing two heavy quarks and another containing two light anti-quarks. This situation suggests that $SU_c(2)$, with moving colour, does not make a good model of nuclear matter.

In summary, the extensions to the string-flip potential model to include the colour-Coulomb interactions did not alter the Q_2 potential significantly enough to achieve binding. This is expected, since it was hypothesized that the colour-hyperfine interactions should play the more significant role [2]. Furthermore, it was shown that the string-flip potential did not give a long-range interaction similar to pion exchange. However, Fig. 7 shows a slight softening of $\bar{U}(R)$ for the $SU_c(2)$ flux-bubble model which perhaps suggests that there might be more to meson exchange than just flux-tube swapping. Finally, when the colour was allowed to move around a rather unphysical situation occurred which suggested that there was perhaps a problem with using $SU_c(2)$ or with the variational wave function itself — perhaps even both. In the next section a more detailed study of the properties of the wave function will be carried out.

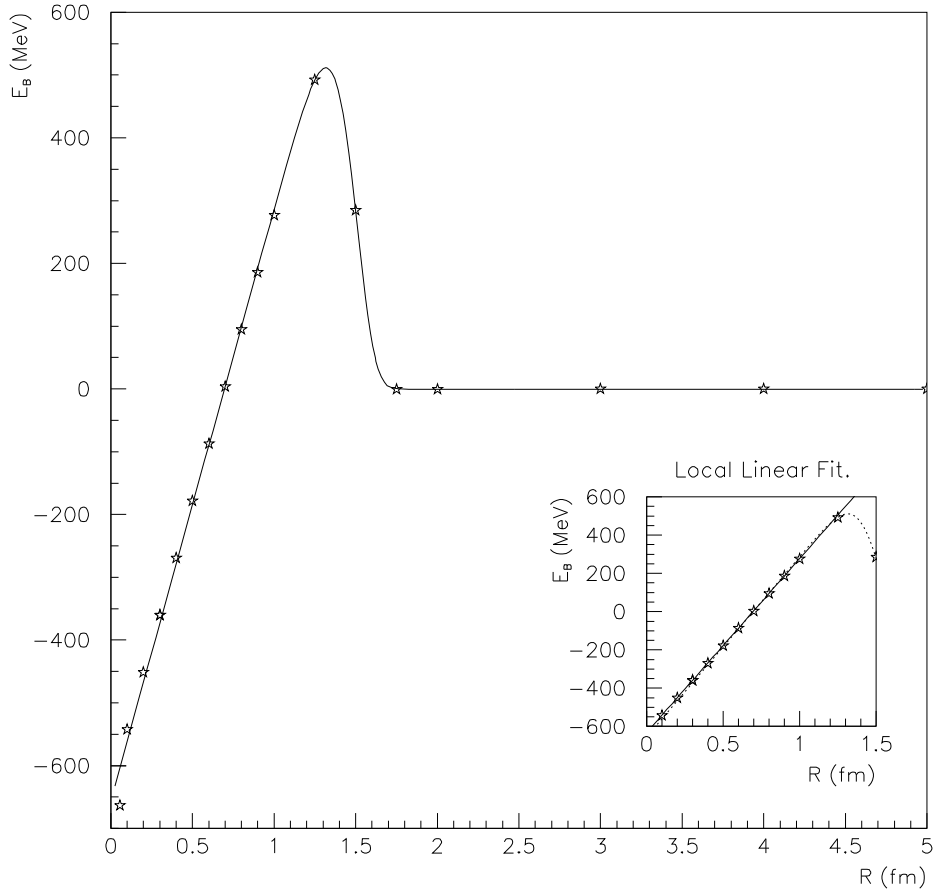


Fig. 8. The Q_2 binding energy curve using the full flux-bubble interaction, *i.e.*, in which the colour is allowed to move around. This curve was parameterized using $u(r)$ given in Fig. 7.

3.2 Back to the $SU_\ell(2)$ String-Flip Potential Model

When the $SU_\ell(2)$ string-flip potential model was investigated in ref. [4] the parameter α in the variational wave function, given by Eq. 4, was fixed by requiring that it minimize the total energy at zero density. Since this could be done analytically it allowed for a reduction in the number of variational parameters used in the Monte Carlo. It was assumed that the constraint would have very little affect on the physics as a function of density since the results varied by about 1% for $1.5 < \alpha < 2.1$, at zero density. The validity of this claim can now be checked more thoroughly by using the Q_2 mini-laboratory.

Fig. 9 shows a plot of the Monte Carlo results, obtained *via* Eqs. 10, 12, and 13, for $\bar{U}(R)$ where α is allowed to vary, $\alpha = 2.00$, and $\alpha = 1.74$. The $\alpha = 2.00$

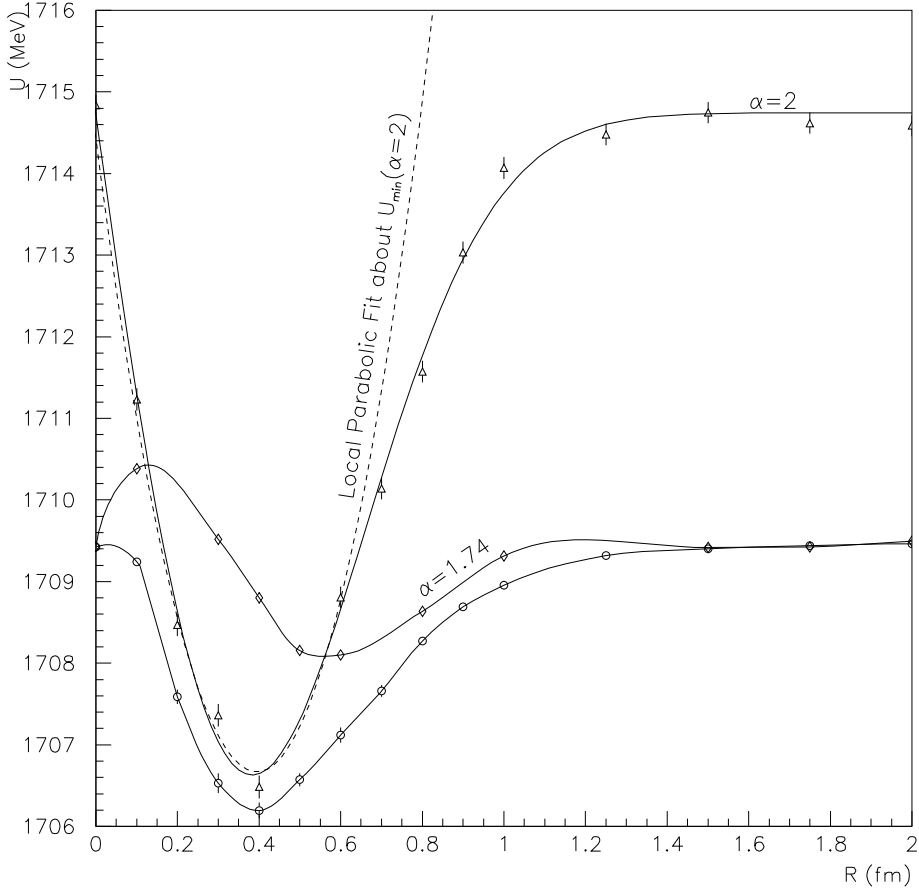


Fig. 9. $\bar{U}(R)$ where α is, allowed to vary, fixed at 2, and fixed at 1.74.

value was used in the old $SU_\ell(2)$ model [4], and $\alpha \approx 1.74$ was the value that minimized $\bar{U}(R)$ at zero separation. The values of $\bar{U}(R)$ at the end points of the curves, from $R = 0 \text{ fm}$ and out to $R = 5 \text{ fm}$, were checked against the analytic solution given by Eq. A.8.

Fig. 10 shows the variations in α and β as a function of R . It would appear from this figure that when α is left free to vary, α and β become extremely correlated. Regardless, looking at the maximum fluctuations about the central values of the parameters α , β , and $\bar{U}(R)$ we have [5] $\alpha \approx (1.88 \pm 0.13)$, $\beta \approx (1.32 \pm 0.05) \text{ fm}$, and $\bar{U}(R) \approx (1710 \pm 4) \text{ MeV}$, which is certainly less than a 1% effect in the energy [4]. However for β it would appear to be an $\mathcal{O}(4)\%$ effect which may have a slight affect on the rate of nuclear swelling.

Surprisingly $\bar{U}(R)|_{\alpha=2}$ gives a much deeper well than expected if α was left as a free parameter: *i.e.*, $D \approx \mathcal{O}(8) \text{ MeV}$ [5]. However, this well is not deep enough to give binding: *i.e.*, a parabolic approximation about the minimum

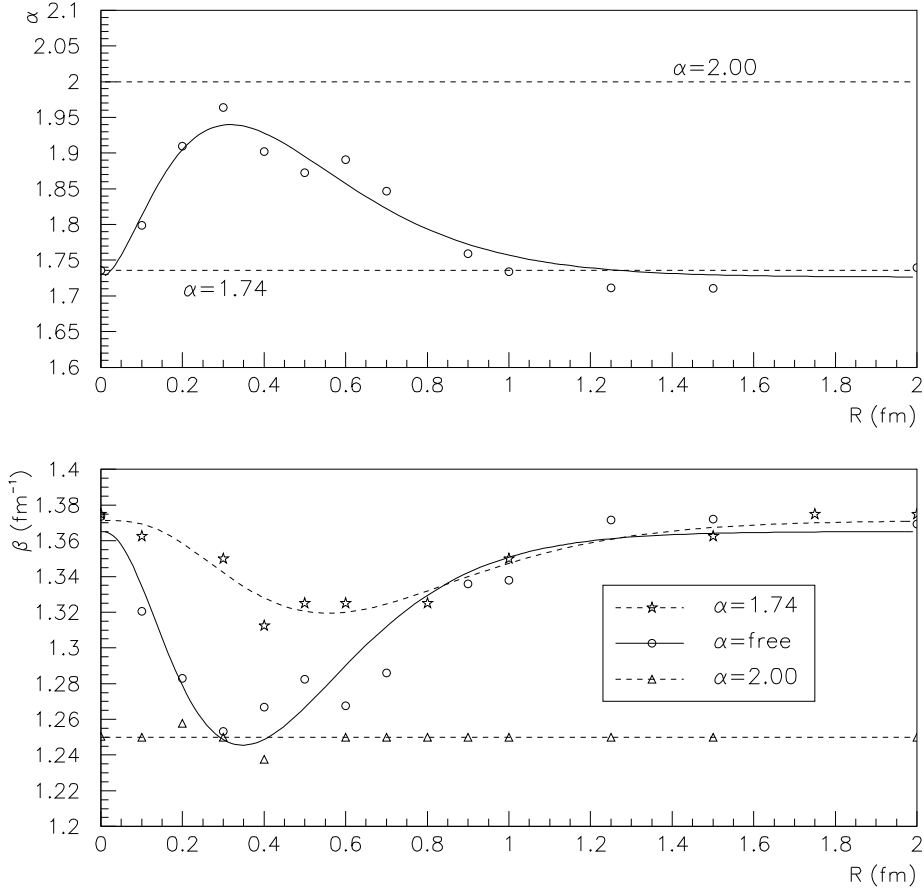


Fig. 10. Graph of $\alpha(R)$ & $\beta(R)$ for the $SU_\ell(2)$ Q_2 -potential model. The dashed lines are for $\alpha = 2.00$ and $\alpha \approx 1.74$. The noise is mainly due to shallow minima on the energy surfaces, $\bar{U}(R)$. The curve on the upper plot and the two upper curves on the lower plot have been parameterized by $a e^{-bR} R^c$, which are provided to guide the eye; they have no physical significance.

(see Fig. 9) requires $\mu_Q \geq \mathcal{O}(15) \text{ GeV}$ [5]. For equal mass constituent quarks this is expected to be a much graver situation.

For certain fixed values of α , $\alpha \approx 1.74$ in Fig. 9 for example, the potential gives a slight short range repulsion. For the range of α values being considered here it is well inside the potential. However, for values of $\alpha \approx 1.0$ the effect becomes quite dramatic.

In general, it is fairly safe to assume that the predicted outcome of the results of past papers [4,2] will not change significantly if α is allowed to vary. However, because the wave function appears to be correlated in both α and β , this seems to suggest that another wave function should be considered in these

models.

3.3 A New Wave Function

The wave function for the old $SU_\ell(2)$ string-flip potential models has been examined. From the analysis it was found that the parameters, α and β , were correlated. Despite this shortcoming, it was thought that this would not have any significant effect on the outcome of the physics predicted by past models, in which α was fixed. However, the purpose of using the Q_2 system was not only to study the properties of this wave function but to ascertain the possibility of devising a new wave function with very few parameters that would take into account the locality of the flux-bubble interactions.

An interesting place to look for such a wave function is in the similarity between the Q_2 mesonic-molecular system and H_2 molecular system. Recall that the key reason for the atomic binding is the screening effect caused by the electrons which are for the most part “localized” in between the protons. This localization is achieved by using a variational wave function that was the superposition of the direct product of two ground state hydrogen atoms, [9,13,14]

$$\Psi \sim e^{-\beta(r_{e_1 P_1} + r_{e_2 P_2})} + e^{-\beta(r_{e_2 P_1} + r_{e_1 P_2})}. \quad (22)$$

Although the Q_2 system is far removed from its H_2 cousin from a dynamical point of view, and the motivations for achieving localization are quite different, this variational wave function does solve the problem for the H_2 system. Therefore, it would seem plausible to make the following *ansatz*:

$$\Psi_{\alpha,\beta} = e^{-\beta^\alpha(r_{\bar{q}_1 Q_1}^\alpha + r_{\bar{q}_2 Q_2}^\alpha)} + e^{-\beta^\alpha(r_{\bar{q}_2 Q_1}^\alpha + r_{\bar{q}_1 Q_2}^\alpha)}. \quad (23)$$

If $\bar{q}_1 Q_1$ and $\bar{q}_2 Q_2$ represent two separate mesons then the first term represents the internal meson interactions while the second term represents the external meson interactions. Notice that the external interactions shut off as the separation, R , between the two heavy quarks becomes large,

$$\lim_{R \rightarrow \infty} \bar{\Psi}(R) = e^{-\beta^\alpha(r_{\bar{q}_1 Q_1}^\alpha + r_{\bar{q}_2 Q_2}^\alpha)} \quad (24)$$

which is the desired property. Furthermore, when the light quarks are close in space, $\Psi(R)$ is considerably enhanced. The effect is that of a “bound-central” wave function.

Using Eq. 9 and Eq. 24 the kinetic energy contribution to the effective potential $U(R)$ in Eq. 10 now becomes [2,5,15]

$$\bar{T} = 2\bar{T}_{-s} - \bar{F}^2, \quad (25)$$

where

$$\begin{aligned}
\bar{T}_{-s} &= \frac{-1}{4m_q} \sum_{\bar{q}} \langle \nabla_{\bar{q}}^2 \ln \Psi \rangle \\
&= \frac{\alpha\beta^\alpha}{4m_q} \left\langle \frac{(\alpha+1)}{\Psi} \left[(r_{\bar{q}_1 Q_1}^{\alpha-2} + r_{\bar{q}_2 Q_2}^{\alpha-2}) e^{-\beta^\alpha(r_{\bar{q}_1 Q_1}^\alpha + r_{\bar{q}_2 Q_2}^\alpha)} \right. \right. \\
&\quad \left. \left. + (r_{\bar{q}_2 Q_1}^{\alpha-2} + r_{\bar{q}_1 Q_2}^{\alpha-2}) e^{-\beta^\alpha(r_{\bar{q}_2 Q_1}^\alpha + r_{\bar{q}_1 Q_2}^\alpha)} \right] \right. \\
&\quad \left. + \frac{\alpha\beta^\alpha}{\Psi^2} [(r_{\bar{q}_1 Q_1}^2 + r_{\bar{q}_1 Q_2}^2 - R^2) r_{\bar{q}_1 Q_1}^{\alpha-2} r_{\bar{q}_1 Q_2}^{\alpha-2} \right. \\
&\quad \left. + (r_{\bar{q}_2 Q_1}^2 + r_{\bar{q}_2 Q_2}^2 - R^2) r_{\bar{q}_2 Q_1}^{\alpha-2} r_{\bar{q}_2 Q_2}^{\alpha-2} \right. \\
&\quad \left. - (r_{\bar{q}_1 Q_1}^{2\alpha-2} + r_{\bar{q}_2 Q_2}^{2\alpha-2} + r_{\bar{q}_2 Q_1}^{2\alpha-2} + r_{\bar{q}_1 Q_2}^{2\alpha-2}) \right] \\
&\quad \left. \times e^{-\beta^\alpha(r_{\bar{q}_1 Q_1}^\alpha + r_{\bar{q}_2 Q_1}^\alpha + r_{\bar{q}_1 Q_2}^\alpha + r_{\bar{q}_2 Q_2}^\alpha)} \right\rangle, \tag{26}
\end{aligned}$$

and

$$\begin{aligned}
\bar{F}^2 &= \frac{1}{2m_q} \sum_{\bar{q}} \langle (\nabla_{\bar{q}} \ln \Psi)^2 \rangle \\
&= \frac{\alpha^2 \beta^{2\alpha}}{2m_q} \left\langle \frac{1}{\Psi^2} \left[(r_{\bar{q}_1 Q_1}^{2\alpha-2} + r_{\bar{q}_2 Q_2}^{2\alpha-2}) e^{-2\beta^\alpha(r_{\bar{q}_1 Q_1}^\alpha + r_{\bar{q}_2 Q_2}^\alpha)} \right. \right. \\
&\quad \left. \left. + (r_{\bar{q}_2 Q_1}^{2\alpha-2} + r_{\bar{q}_1 Q_2}^{2\alpha-2}) e^{-2\beta^\alpha(r_{\bar{q}_2 Q_1}^\alpha + r_{\bar{q}_1 Q_2}^\alpha)} \right] \right. \\
&\quad \left. + [(r_{\bar{q}_1 Q_1}^2 + r_{\bar{q}_1 Q_2}^2 - R^2) r_{\bar{q}_1 Q_1}^{\alpha-2} r_{\bar{q}_1 Q_2}^{\alpha-2} \right. \\
&\quad \left. + (r_{\bar{q}_2 Q_1}^2 + r_{\bar{q}_2 Q_2}^2 - R^2) r_{\bar{q}_2 Q_1}^{\alpha-2} r_{\bar{q}_2 Q_2}^{\alpha-2}] \right. \\
&\quad \left. \times e^{-\beta^\alpha(r_{\bar{q}_1 Q_1}^\alpha + r_{\bar{q}_2 Q_1}^\alpha + r_{\bar{q}_1 Q_2}^\alpha + r_{\bar{q}_2 Q_2}^\alpha)} \right\rangle. \tag{27}
\end{aligned}$$

It is interesting to note, and it also serves as a good check of the computation, that in the large R limit the kinetic energy corresponds exactly to the kinetic energy for the old wave function in the same limit:

$$\lim_{R \rightarrow \infty} \bar{T}(R) = \frac{\alpha\beta^\alpha}{2m_q} \left\langle (\alpha+1) (r_{\bar{q}_1 Q_1}^{\alpha-2} + r_{\bar{q}_2 Q_2}^{\alpha-2}) - \alpha\beta^\alpha (r_{\bar{q}_1 Q_1}^{2\alpha-2} + r_{\bar{q}_2 Q_2}^{2\alpha-2}) \right\rangle$$

$$= \frac{\alpha\beta^\alpha}{2m_q} \left\langle \sum_{i=1}^2 [\alpha(1 - (\beta r_{\bar{q}_i Q_i})^\alpha) + 1] r_{\bar{q}_i Q_i}^{\alpha-2} \right\rangle, \quad (28)$$

cf. Eq. 15. Also direct evaluation of the RHS leads to (assuming Ψ is properly normalized)

$$\lim_{R \rightarrow \infty} \bar{T}(R) = \frac{g_T(\alpha)}{m_q} \beta^2, \quad (29)$$

which is just the kinetic term for the analytic solution given by Eq. A.1.

The Monte Carlo computations that were done, using the pseudo-hydrogen wave function, $\tilde{\Psi}_H$ (*i.e.*, Eq. 12) in § 3.1, have been repeated here for the pseudo-hydrogen-molecular wave function, $\tilde{\Psi}_{H_2}$ (*i.e.*, Eq. 23), and are shown in Figs. 11 and 12.

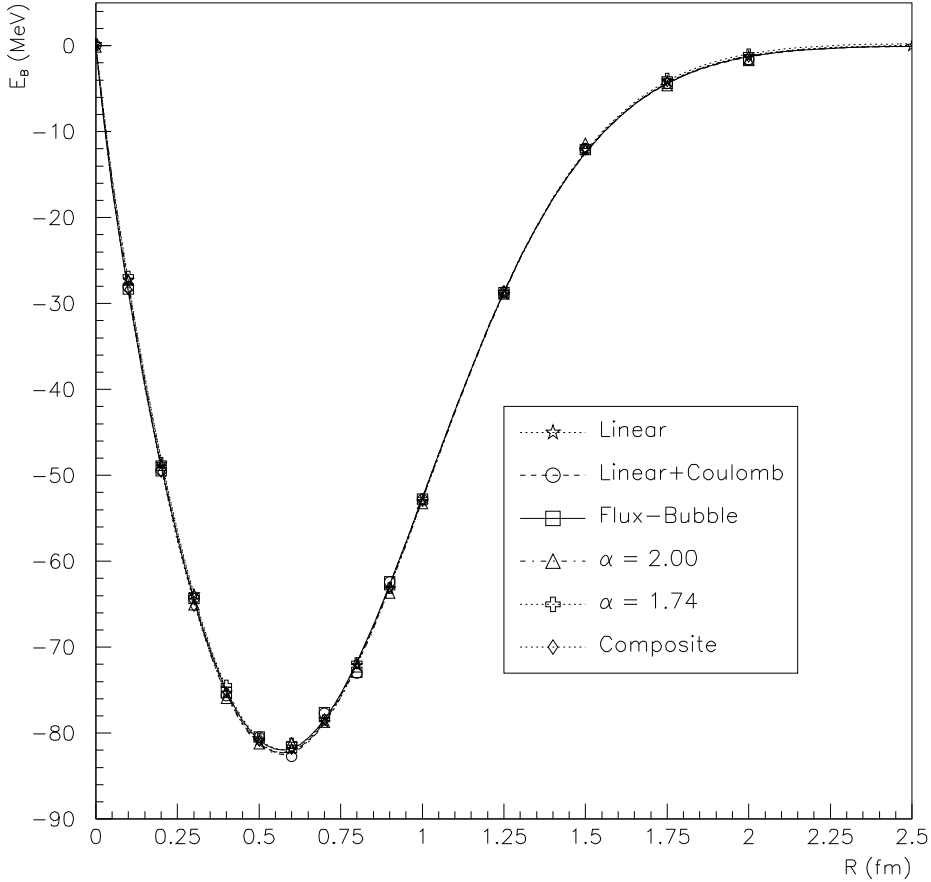


Fig. 11. The binding energy, $E_B(R)$, for the Q_2 system as function of heavy quark separation for a linear, a linear-plus-Coulomb, and a flux-bubble potential model. Also shown, are the curves for $\alpha = 2.00$ and 1.74 , and the composite model discussed in § 4. The curves in these plots have been parameterized by $u(r)$ given in Fig 7.

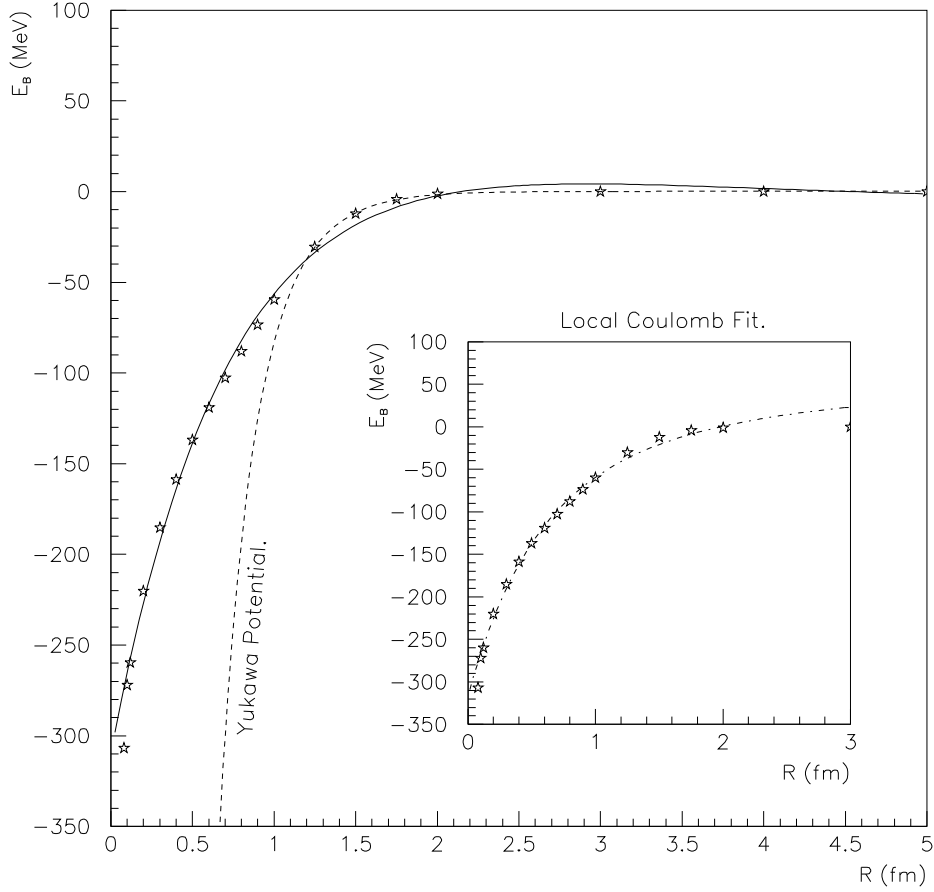


Fig. 12. The Q_2 binding energy curve using the full flux-bubble interaction, *i.e.*, in which the colour is allowed to move around. This curve was parameterized using $u(r)$ given in Fig. 7.

It can be immediately seen, that there is a dramatic contrast between the figures for $\tilde{\Psi}_H$ and $\tilde{\Psi}_{H_2}$. For the plots in Fig. 11 the wells are much deeper and the binding energy constraints have come down considerably: *i.e.*, *via* table A.2, we have

$$\bar{D} \approx (82.46 \pm 0.49) \text{ MeV}, \quad (30)$$

and

$$\mu_Q \gtrsim (660 \pm 24) \text{ MeV}. \quad (31)$$

These potentials are now strong enough to bind the more massive quarks, such as c and b .

The effective Yukawa masses, *i.e.*,

$$\bar{m}_{\text{ex}} \approx (575 \pm 32) \text{ MeV}, \quad (32)$$

via table A.3, are roughly the same order of magnitude as the $\tilde{\Psi}_H$ case, Eq. 21, but with a slightly less dramatic softening effect on the tail of the potential. However, these masses are still too large to explain pion exchange.

Also included in Fig 11, are plots for α fixed at 2 and 1.74. Here, the effects do not appear as drastic as with the old wave function since the depth of the well simply overwhelms them.⁴ Therefore, any new model of nuclear matter that incorporates $\tilde{\Psi}_{H_2}$ should run into no difficulties by fixing α .

The final figure, Fig. 12, of the flux-bubble model with moving colour is quite intriguing. The anomalies in Fig. 8 have disappeared; the light quarks have not drifted away as an isolated pair to leave a linear potential between the heavy quarks. In fact, there is no more linearity inside the well. Naïvely, this seems to suggest that the problem was with the wave function and not $SU_c(2)$. However, this is not quite the case, since the old wave function gives an interior well depth which twice as deep. Therefore, it is energetically more favourable for the Q_2 system to dissociate into two isolated mesons; one with two light quarks and the other with two heavy ones.

An attempt was made to find the shape of the interior of the well, and it was found that it fitted to a Coulomb potential of the form,

$$V_C(r) = -\frac{a}{r} \left(1 - e^{-\beta r}\right) + V_\infty \quad (33)$$

(see insert in Fig. 12), with $a \approx (135.5 \pm 2.9) \text{ MeV fm}$, $\beta \approx (2.844 \pm 0.048) \text{ fm}^{-1}$, $V_\infty \approx (68.3 \pm 2.6) \text{ MeV}$. The term in the brackets was included to mimic the overlap between the charge distributions of two mesonic systems. In terms of α_s , the hyperfine constant for this region of the potential is

$$\alpha_{Q_2} \approx (6.86 \pm 0.15)\alpha_s. \quad (34)$$

The interior part of the potential is quite deep and bottoms out at $\mathcal{O}(-270) \text{ MeV}$, at which point the $-\alpha_s/r$ term for the heavy quarks kicks in (*i.e.*, for $R \leq 0.1 \text{ fm}$). The exterior part of the potential fits to a Yukawa potential with $m_{\text{ex}} \approx (612 \pm 32) \text{ MeV}$ (*via* table A.3).

4 Discussion

Various aspects of model building for nuclear matter have been examined in the context of the Q_2 system. The ramifications of these investigations will now be discussed.

⁴ In fact, almost “all” of the curves are independent of the details of the potential.

Perhaps the most important result is the new variational wave function, Eq. 23. This new wave function made a large change in the depth of the Q_2 potential well. The depth increased by a factor of 27, deep enough to bind heavy quarks: *i.e.*, $m_q \gtrsim \mathcal{O}(m_c)$. The wave function also fulfills the requirement of handling local flux-bubble interactions, which becomes apparent when looking at the “before” and “after” pictures (of moving colour) in Figs. 8 and 12, respectively. Therefore, in $SU_\ell(2)$ for a many quark system this would suggest the following *ansatz*:

$$\Psi \sim \text{Perm}|\tilde{\Psi}_H(r_{p_i p_j})| \prod_{\text{colour}} |\Phi(r_{p_k})| \quad (35)$$

where

$$\tilde{\Psi}_H(r_{p_i p_j}) = e^{-\left(\beta r_{p_i p_j}\right)^\alpha}, \quad (36)$$

$\text{Perm}|\tilde{\Psi}_H(r_{p_i p_j})|$ is a totally symmetric pseudo-hydrogen wave function and $|\Phi(r_{p_k})|$ is a totally antisymmetric Slater wave function. (For the full three-quark system a similar wave function would apply.) This does not necessarily mean that this wave function would lead to nuclear binding, since binding was only achieved for relatively very heavy quarks in the Q_2 system. However, given the order of magnitude of increase in the Q_2 well depth it would seem quite plausible that it might be a strong enough effect to produce a shallow well in the nuclear-binding-energy curve. A simple test would be to consider $SU_\ell(2)$ with just a string-flip potential, with α fixed, in which case scaling is restored and the Monte Carlo becomes quite straightforward to do.

The flux-bubble model proved quite successful at combining colour-Coulomb interactions with flux-tube interactions. Although these interactions, in general, had very little affect on the Q_2 system it was useful in demonstrating that extending the flux-tube model to include local perturbative QCD interactions can be done. Furthermore, it was not surprising that this had very little effect, as it was hypothesized [2,5,16] that the hyperfine interactions should play the more dominant role. Therefore, it would prove most interesting to investigate the effect of adding more perturbative interactions to the Q_2 system. With the addition of $SU_c(3)$ this would lead to a more realistic model of mesonic molecules which perhaps could be tested in the laboratory.

When the $SU_\ell(2)$ flux-bubble model with moving colour was considered, the results were quite interesting; the Q_2 system dissociated into one light and one heavy meson. However, this system is not physical. A more useful model, would be to consider the heavy quarks as a composite of two light quarks and use $SU_c(3)$ instead. In this case it would not be possible for a flux-tube to form between the two heavy quarks, causing the system to dissociate. For this

“composite” model, the $\lambda_{p_i p_j}$'s of potential Eq. 16 become

$$\lambda_{p_i p_j} = \begin{cases} \frac{1}{3} & \text{if } p_i p_j \in \{bb, \bar{B}\bar{B}\} \\ \frac{1}{6} & \text{if } p_i p_j \in \{b\bar{G}, \bar{B}g\} \\ -\frac{1}{6} & \text{if } p_i p_j \in \{b\bar{B}, g\bar{G}\} \\ -\frac{1}{3} & \text{if } p_i p_j \in \{bg, \bar{B}\bar{G}\} \\ -\frac{4}{3} & \text{if } p_i p_j \in \min\{q_r \bar{q}_s\} \end{cases} \quad , \quad (37)$$

such that $rg \sim \bar{B}$ and $rb \sim \bar{G}$ for the composite states, $bb \sim gg$ and $\bar{B}\bar{B} \sim \bar{G}\bar{G}$. Indeed, when this is done, one obtains a more meaningful curve. See Fig. 11. Unfortunately, this model yields no improvements in the overall depth of the well.

Curiously if the heavy quarks were considered to be a composite of two light u quarks then

$$\mu_{Q \supseteq \{uu\}} / \mu_{\min} \approx \mathcal{O}(0.6) \quad (38)$$

which is getting closer to binding, but is not quite sufficient. This would seem to suggest that perhaps slight nucleon deformations [6] would help to enhance binding. Therefore, an interesting possibility would be to consider a many-body $SU_\ell(2)$ or $SU_\ell(3)$ flux-bubble model in which there is an imbalance between the quark and anti-quark masses.

One might also want to consider relativistic effects. However, it is found that this appears to slightly exacerbate the problem. Fig. 7 shows the case for the old wave function using the relativistic approximation⁵

$$\sum_{\min\{Q\bar{q}\}} [\nabla_{\bar{q}}^2 + (m_q + \sigma r_{Q\bar{q}})^2] \Psi = U^2(R) \Psi. \quad (39)$$

A similar result is expected for the case of the new wave function, resulting in a comparatively minor change in the well depth.

From our analysis of the Q_2 system, it would appear that the most significant find is that of the newly proposed many-body wave function for nuclear matter, Eq. 35. For the Q_2 system, this caused a dramatic change in the depth of its potential well. It is also expected to have a similar effect for the $SU_\ell(2)$ $q\bar{q}$ model of nuclear matter [4]. In fact, it may be enough of an effect to produce nucleon binding. Further enhancements are expected by going to the full qqq nucleon model in which slight nuclear deformations may contribute. A less ambitious version would be to consider a $Q\bar{q}$ nucleon model, using $SU_\ell(2)$,

⁵ This result was obtained from the Dirac equation by performing an approximation similar to that of Hartree and Fock (*e.g.*, [17]), assuming the flux-tube interaction is a Lorentz scalar.

in which $m_Q \approx 2m_q$. If no binding is obtained, then the next step would be to study effects of adding flux-bubble interactions. In particular, the colour-hyperfine interaction which is shown by linked cluster expansion models to play a significant role nuclear processes [16]. With slight nuclear deformations this may be enough produce the contact interactions which are responsible for nuclear binding [18].

5 Conclusions

The Q_2 system has proven to be a very useful aid for trying to sort out the complexities of model building for nuclear matter. The details of the mechanics, from wave functions to dynamics to practical computing methods, of the flux-bubble model have now been thoroughly investigated. It appears that the flux-bubble model may prove to be very successful, not only for modeling nuclear matter but also for modeling mesonic molecules as well.

Acknowledgements

This work was supported by NSERC. The Monte Carlo calculations were performed on an 8 node DEC 5240 UNIX CPU farm, using Berkeley Sockets (TCP/IP) [19]. The computing facilities were provided by Carleton University's, Department of Physics, OPAL, CRPP, and THEORY groups. We would like to thank M.A. Doncheski, H. Blundell, M. Jones, and J.S. Wright for useful discussions.

A Analysis

This appendix contains a summary of the analysis done for the models given in sections 3.1 through 3.3 of this paper.

All of the results of these sections make use of the general potential Eq. 18. For $\bar{U}(R)$, as defined by Eq. 10, some analytical results were obtainable where the Q_2 system effectively dissociates into two isolated meson systems. For all of the plots this occurs at $\bar{U}(\infty)$, and for the linear and linear-plus-Coulomb plots this also occurs at $\bar{U}(0)$. In these regions, the analytic expression is given by (*cf.* [4])

$$E_{free} = 2 \left[\frac{g_T(\alpha)}{2\mu} \beta^2 + \sigma \left(\frac{g_L(\alpha, \beta)}{\beta} - g_0(\alpha, \beta) r_0 \right) \right]$$

$$-\frac{3}{4} \alpha_s \left(g_C(\alpha, \beta) \beta - \frac{(1 - g_0(\alpha, \beta))}{r_0} \right) \Big], \quad (\text{A.1})$$

where

$$g_L(\alpha, \beta) = [1 - P(4/\alpha, 2(\beta r_0)^\alpha)] g_L(\alpha), \quad (\text{A.2})$$

$$g_C(\alpha, \beta) = P(2/\alpha, 2(\beta r_0)^\alpha) g_C(\alpha), \quad (\text{A.3})$$

$$g_0(\alpha, \beta) = 1 - P(3/\alpha, 2(\beta r_0)^\alpha), \quad (\text{A.4})$$

such that

$$g_T(\alpha) = \frac{\alpha^2 2^{\frac{2}{\alpha} - 2} \Gamma(2 + 1/\alpha)}{\Gamma(3/\alpha)}, \quad (\text{A.5})$$

$$g_L(\alpha) = \frac{\Gamma(4/\alpha)}{2^{\frac{1}{\alpha}} \Gamma(3/\alpha)}, \quad (\text{A.6})$$

$$g_C(\alpha) = \frac{\Gamma(2/\alpha)}{2^{-\frac{1}{\alpha}} \Gamma(3/\alpha)}, \quad (\text{A.7})$$

$P(a, z) = 1 - \Gamma(a, z)/\Gamma(a)$, and $\Gamma(a, z)$ is the incomplete gamma function [20,21]. In the limits as $r_0 \rightarrow 0$ and $r_0 \rightarrow \infty$ Eq. (A.1) reduces to solutions for the purely linear,

$$E_{free} \xrightarrow{r_0 \rightarrow 0} 2 \left(\frac{g_T(\alpha)}{2\mu} \beta^2 + g_L(\alpha) \frac{\sigma}{\beta} \right), \quad (\text{A.8})$$

and purely Coulomb,

$$E_{free} \xrightarrow{r_0 \rightarrow \infty} 2 \left(\frac{g_T(\alpha)}{2\mu} \beta^2 - \frac{3}{4} \alpha_s g_C(\alpha) \beta \right), \quad (\text{A.9})$$

cases, respectively. Table A.1 gives a summary of the Monte Carlo vs. analytic results. The results for the linear and linear-plus-Coulomb potentials, at $R = 0 \text{ fm}$ and $R = 5 \text{ fm}$ (*i.e.*, $\approx \infty$), were checked against Eqs. A.8 and A.1, respectively. The flux-bubble case, at $R = 5 \text{ fm}$, was verified using Eq. A.1. The minima of the analytic expressions, which were used to verify the aforementioned models, were found *via* the `FindMinimum[...]` routine in Mathematica [20].

The binding energy of the Q_2 system can be estimated by doing a local parabolic fit [12] about the minimum of $\bar{U}(R)$: *i.e.*, by fitting

$$y(r) = \mathcal{C}(r - r_0)^2 - \mathcal{D} \quad (\text{A.10})$$

such that $\mathcal{C} = \mu_Q \omega^2 / [2(\hbar c)^2]$, where μ_Q is the reduced mass of the heavy

Table A.1

Monte Carlo (MC) vs. analytic results for Figs. 7, 8, 11 and 12.

| Method | | Fig. | R (fm) | E_{free} (MeV) | α | β (fm ⁻¹) |
|----------|-------------|------|-------------|----------------------|----------|-----------------------------|
| Analytic | Eq. A.8 | n.a. | 0/ ∞ | 1709.61 | 1.75 | 1.37 |
| MC | Linear | 7 | 0 | 1709.424 \pm 0.038 | 1.74 | 1.37 |
| | | | 5 | 1709.492 \pm 0.044 | 1.72 | 1.38 |
| | | 11 | 0 | 1709.647 \pm 0.032 | 1.77 | 1.36 |
| | | | 5 | 1709.485 \pm 0.032 | 1.75 | 1.36 |
| Analytic | Eq. A.1 | n.a. | 0/ ∞ | 1527.07 | 1.74 | 1.37 |
| MC | Linear | 7 | 0 | 1527.171 \pm 0.029 | 1.78 | 1.36 |
| | | | 5 | 1527.171 \pm 0.029 | 1.78 | 1.36 |
| | Coulomb | 11 | 0 | 1527.884 \pm 0.041 | 1.74 | 1.34 |
| | | | 5 | 1527.884 \pm 0.041 | 1.74 | 1.34 |
| MC | Flux-Bubble | 7 | 5 | 1526.974 \pm 0.032 | 1.74 | 1.36 |
| | | 8 | 5 | 1527.884 \pm 0.041 | 1.74 | 1.34 |
| | | 11 | 5 | 1527.884 \pm 0.041 | 1.74 | 1.34 |
| | | 12 | 5 | 1527.173 \pm 0.062 | 1.68 | 1.40 |

quarks. Therefore, the binding energy is simply

$$E_h^\nu = (\nu + \frac{1}{2})\hbar\omega - \mathcal{D}, \quad (\text{A.11})$$

which implies

$$\mu_Q \geq \mu_{\min} \equiv \frac{\mathcal{C}(\hbar c)^2}{2\mathcal{D}^2} \quad (\text{A.12})$$

in order to obtain binding. Table A.2 shows the results for the parabolic fits to the $\bar{U}(R)$'s in Fig. 7.

The asymptotic parts of the $\bar{U}(R)$'s were fitted to a Yukawa potential of the form

$$V_Y(r) = -2f^2 \frac{e^{-\mu r}}{r}. \quad (\text{A.13})$$

Table A.3 summarizes the Yukawa fits for all of the models.

Table A.2

Results for local parabolic fitting about the minima of the plots in Figs. 7 and 11.

| Model | Fig. | $\mathcal{C} (MeV/fm^2)$ | $r_0 (fm)$ | $\mathcal{D} (MeV)$ | $\mu_{\min} (GeV)$ |
|---------------------|------|--------------------------|---------------------|---------------------|--------------------|
| Linear | 7 | 29.8 ± 1.5 | 0.4174 ± 0.0056 | 3.268 ± 0.058 | 54.3 ± 3.3 |
| | 11 | 234.8 ± 8.0 | 0.5288 ± 0.0057 | 82.55 ± 0.49 | 671 ± 24 |
| Linear + Coulomb | 7 | 28.7 ± 1.4 | 0.4134 ± 0.0045 | 3.098 ± 0.060 | 58.2 ± 3.6 |
| | 11 | 230.3 ± 8.0 | 0.5833 ± 0.0058 | 82.60 ± 0.49 | 657 ± 24 |
| Flux-Bubble | 7 | 20.0 ± 1.0 | 0.4614 ± 0.0034 | 2.783 ± 0.042 | 50.3 ± 2.9 |
| | 11 | 226.8 ± 8.0 | 0.5840 ± 0.0059 | 82.24 ± 0.49 | 653 ± 24 |

Table A.3

Results for asymptotic Yukawa fits of the plots in Figs. 7, 11, and 12, where $m_{\text{ex}} = \hbar c \mu$.

| Model | Fig. | $f^2 (MeV fm)$ | $\mu (fm^{-1})$ | $m_{\text{ex}} (MeV)$ |
|----------------|------|-----------------|-----------------|-----------------------|
| Linear | 7 | 2.49 ± 0.20 | 3.23 ± 0.21 | 637 ± 41 |
| | 11 | 27.3 ± 2.7 | 2.97 ± 0.16 | 586 ± 32 |
| Linear+Coulomb | 7 | 2.0 ± 2.2 | 3.0 ± 3.5 | 590 ± 690 |
| | 11 | 25.9 ± 2.7 | 2.89 ± 0.16 | 570 ± 32 |
| Flux-Bubble | 7 | 1.8 ± 2.3 | 2.4 ± 3.5 | 470 ± 690 |
| | 11 | 25.9 ± 2.7 | 2.89 ± 0.16 | 570 ± 32 |
| | 12 | 30.3 ± 2.1 | 3.10 ± 0.11 | 612 ± 32 |

References

- [1] G. Peter Lepage, *The Fall and Rise of Lattice QCD*, seminar at the Ottawa-Carleton Institute for Physics, Feb. 5th 1996.
- [2] M.M. Boyce and P.J.S. Watson, *Nuc. Phys.* **A580** (1994) 500.
- [3] C.J. Horowitz and J. Piekarewicz, *Nucl. Phys.* **A536** (1991) 669-696.
- [4] P.J.S. Watson, *Nucl. Phys.* **A494**, (1989) 543.
- [5] M.M. Boyce, **String Inspired QCD and E₆ Models**, *Ph.D. thesis (1996)*,

Carleton U., Dept. of Physics, 1125 Colonel By Dr., Ottawa, ONT, Canada, K1S-5B6; hep-ph/9609433.

- [6] J. Carlson, J. Kogut, and V.R. Pandharipnade, Phys. Rev. **D27** (1983) 233.
- [7] M.M. Boyce and P.J.S. Watson, **SU(3) String-Flip Potential Models and Nuclear Matter**, “MRST ’94,” conference, “What Next? Exploring the Future of High-Energy Physics,” Ed: J.R. Cudell, K.R. Dienes, and B. Margolis, World Scientific (1994); hep-ph/9501397.
- [8] John Weinstein and Nathan Isgur, Phys. Rev. **D41**, (1990) 2236.
ibid, Phys. Rev. **D27**, (1983) 588.
ibid, Phys. Rev. Lett., (1982) 659.
- [9] Leonard I. Schiff, **Quantum Mechanics**, 2nded, McGraw Hill (1968).
- [10] N. Metropolis, A.W. Rosenbluth, M.N. Rosenbluth, A.H. Teller, and E. Teller, J. Chem. Phys. **21** (1953) 1087.
- [11] M.M. Boyce, **The Distributed Minimization Algorithm**, *in preparation*.
- [12] Siegfried Flügge, **Practical Quantum Mechanics I**, Springer-Verlag, Berlin, Heidelberg, New York (1971).
- [13] B.H. Bransden and C.J. Joachain, **Physics of Atoms and Molecules**, Longman Group Limited (1983).
- [14] W. Heitler and F. London, Z. Physik **44**, (1927) 455.
- [15] D. Ceperley, G.V. Chester, and M.H. Kalos, Phys. Rev. **B16** (1977) 3081.
- [16] Mohammad Nzar and Pervez Hoodbhoy, Phys. Rev. **C42** (1990) 1778.
- [17] D. Liberman, J.T. Waber and Don T. Cormer, Phys. Rev. **A27**, (1986) 137.
- [18] Philip J. Siemens and Aksel S. Jensen, **Elements of Nuclei**, Many-Body Physics with the Strong Interaction, *Lecture Notes and Supplements in Physics*, Addison-Wesley (1987).
- [19] W. Richard Stevens, **UNIX Network Programmings**, PTR Prentice Hall (1990).
- [20] Stephen Wolfram (*Wolfram Research, inc: into@wri.com*), **Mathematica**, *A System for Doing Mathematics by Computer*, 2nd ed, Addison-Wesley (1991).
- [21] Milton Abramowitz and Irene A. Stegun, **Handbook of Mathematical Functions**, *with Formulas, Graphs, and Mathematical Tables*, Dover Publications Inc., New York (1972).